frontiers | Frontiers in Earth Science

TYPE Original Research
PUBLISHED 25 August 2022
DOI 10.3389/feart.2022.973528

OPEN ACCESS

EDITED BY
Changdong Li,
China University of Geosciences
Wuhan, China

REVIEWED BY
Shenghua Cui,
Chengdu University of Technology,
China
Ming Zhang,
China University of Geosciences
Wuhan, China

*CORRESPONDENCE
Hufeng Yang,
yanghf@swjtu.edu.cn

SPECIALTY SECTION
This article was submitted to
Geohazards and Georisks,
a section of the journal
Frontiers in Earth Science

RECEIVED 20 June 2022
ACCEPTED 25 July 2022
PUBLISHED 25 August 2022

CITATION
Yang H, Xing B, He J, Jiang H and
Cheng Q (2022), The formation
mechanism and failure mode of a talus
slope induced by rockfalls in Nayong
County, Southwest China.
Front. Earth Sci. 10:973528.
doi: 10.3389/feart.2022.973528

The formation mechanism and failure mode of a talus slope induced by rockfalls in Nayong County, Southwest China

Hufeng Yang[1]*, Bencong Xing[1], Jiangkun He[1], Hu Jiang[2] and Qiang Cheng[3]

[1]Faculty of Geosciences and Environmental Engineering, Southwest Jiaotong University, Chengdu, China, [2]Kunming Survey, Design and Research Institute Co, Ltd. of CREEC, Kunming, China, [3]Sichuan Highway Planning, Survey, Design and Research Institute Ltd, Chengdu, China

Hillslope processes and mass movement are key issues in the analysis and evaluation of geological disasters in mountainous regions. A rockfall-dominated talus slope exhibits a typical outcrop–talus slope system as the product of detached boulders and rock fragments. The Zongling rockfall zone is one of the most active outcrop–talus slope systems in southwest China, and it provides a representative case study on the assessment of rockfall hazards at the base of talus slopes. In this article, the formation mechanism and failure mode of this rock-talus system were studied using field investigation, remote sensing image analysis, and numerical simulation. The findings reveal that the lithology and rock mass structure of the study site are controlling factors for outcrop retreat and the progressive development of talus deposits. This process is intensified by rainfall and mining activities. Boulder accumulation on the platform at the middle section of the talus slope serves as top loading for the slope mechanical system. During the boulder–ground interaction, the rockfall impact acts as toe cutting to change the geometry and mechanical balance of the talus slope. It was found that toe cutting significantly influenced the slope stability, which led to a decrease in the antisliding force of the slope. The slope failure induced by rockfalls occurred with the combined effect of top loading and toe cutting on this talus slope. During rockfall prevention and mitigation in this region, the government and residents should consider the geodisaster chain, as this relates to the impact of rockfall on talus slopes, in addition to the risk of damage due to the rockfall trajectory.

KEYWORDS

rockfall, talus slope, formation mechanism, failure mode, geodisaster chain

Introduction

A rockfall-dominated talus slope exhibits a typical outcrop–talus slope system as the product of detached boulders and rock fragments from the outcrop in mountains. The evaluation of the talus slope is one of the most important slope surface processes on the exposed hard rocks in mountainous regions (Statham, 1976; Evans and Hungr, 1993; De Blasio and Sæter, 2015). Recently, research on rockfall activity in outcrop–talus slope systems has been conducted mainly for the European Alps (Jomelli and Francou, 2000; McCarroll et al., 2001; Otto and Sass, 2005; Sanders, 2010; Sanders et al., 2014; Colucci et al., 2016; Vehling et al., 2017; Messenzehl et al., 2018; Hendrickx et al., 2020), the Japanese Alps (Imaizumi et al., 2020), and some mountains in the UK (Curry and Morris, 2004), North America (Veilleux et al., 2020; Collins et al., 2022), and the Tibetan Plateau (Wan et al., 2021).

Generally, talus slope instability is the result of slope angle evaluation when the slope angle is beyond the natural angle of repose for rock fragments. However, external factors also influence slope stability, such as rainfall, freezing–thawing, and dynamic load from earthquakes or engineering activities (Matsuoka and Sakai, 1999; Zhang et al., 2010; Xing et al., 2019; Imaizumi et al., 2020). Rockfalls from the outcrop are the source material for the formation of talus slopes. Additionally, rockfall impact plays an important role in changes to slope geometry and slope instability (Gerber and Scheidegger, 1974; Statham, 1976; Sass and Krautblatter, 2007; Hale et al., 2009; De Blasio and Sæter, 2015). For example, on 6 May 2011, a 5,800 m^3 rockfall of dolostone detached from the flank of a gorge in the upper part of a mountain in Austria (Central Alps) and triggered a medium-scale avalanche on the talus slope (Sanders et al., 2014). Considering the global climate change, the assessment of rockfall hazards at the base of talus slopes in outcrop–talus slope systems has become a research hotspot in high-altitude and high-latitude regions.

The Zongling rockfall zone is one of the most active outcrop–talus slope systems in southwest China (Gong and Zhao, 2009). There are 12 rockfall-dominated talus slopes in this rockfall zone, which is located in western Nayong County (Figure 1). Since 2000, there have been more than 20 occurrences of rockfall geodisaster events in this rockfall zone (Cheng et al., 2019). One such instance was a catastrophic landslide that occurred in Zuojiaying village on 3 December 2004, resulting in 39 casualties and five missing persons (Liu et al., 2004; Chen et al., 2006; Wu et al., 2006). In another occurrence in the early morning of 6 June 2015, a large-scale rockfall occurred at Zuojiaying, resulting in three casualties (Cheng et al., 2019). For the mechanism and risk assessment of rockfalls in Zongling Town, several scholars have carried out field investigations and numerical analyses. In 2013, Tan (2013) evaluated the deformation failure mechanism and stability of a high slope at Zongling Town and proposed the toppling failure mode. Subsequently, Jiao (2015) delimited the maximum influence range of rockfalls based on the analysis of a typical collapse zone. Since then, Cheng et al. (2019) have divided rockfall zones into accumulation areas, severely affected areas, and evacuation areas. Shi (2019) has used Zongling Town as an example to conduct the risk assessment of geological hazards for rural areas. Wang (2019) qualitatively analyzed the slope deformation induced by a mined-out area (coal mining) at the bottom of the Mazongling slope.

Recently, most research has focused on rockfall events in the Zongling rockfall zone but not specifically on the talus slope dominated by rockfalls. This study focuses on the instability of a talus slope induced by rockfalls: rockfall-dominated talus slope No. 11 (Figure 1). The formation mechanism and failure mode of this rock-talus system were studied by field investigation, remote

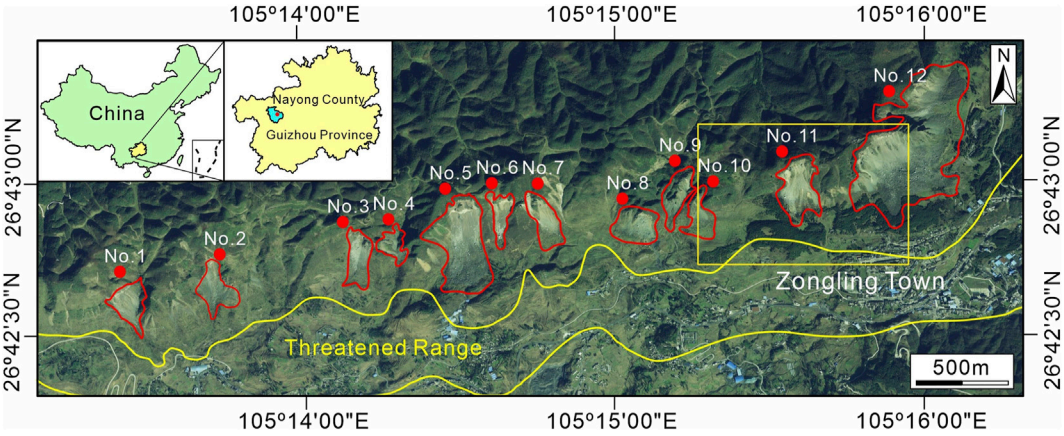

FIGURE 1
Distribution of 12 rockfall-dominated talus slopes in the Zongling rockfall zone (image source: Google Earth).

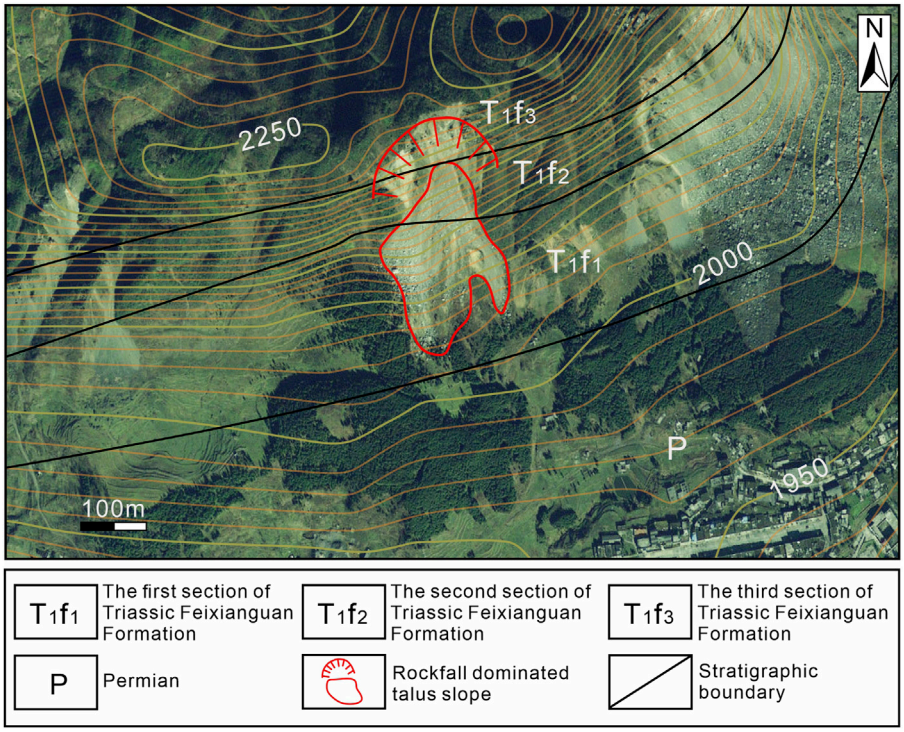

FIGURE 2
Topographic and stratigraphic map of the study site (image source: Google Earth).

sensing image analysis, and numerical simulation. The results indicate that the main reasons for talus slope failure are top loading from boulder accumulation on the slope top, and toe cutting by rockfall impact at the slope toe. Finally, a failure mode for the rockfall-dominated talus slopes was developed in a way that considers the coupling effect of top loading and toe cutting from rockfall. The findings and proposed mode introduced by this study are of practical significance for the prevention and mitigation of rockfall geodisasters in this region.

Geological environmental conditions of the study site

Geomorphology

The Zongling rockfall zone presents with a northeastern trend, with its slope facing south. The terrain is generally high in the east and low in the west, with an altitude of 1,623–2,000 m. The highest point is in the east. To the north of the cliff, the mountains are undulating: the terrain is generally high in the south and low in the north, with an altitude of 2,100–2,334.5 m. The steep cliff has a slope of 50–80° and a height of 100–300 m. The lower slope of the steep cliff becomes gentle, with a slope of about 30–45°. Hilly farmland and local villagers are mostly distributed along the foot of the gentle slope or by the flat mountain highland (Shen and Li, 2015). The study site is located 500 m northwest of Zongling Town. Here, the rockfall source area is a steep cliff with a slope angle of 60–80°, and the talus slope becomes gentler with a slope angle of 35–45°. The relative height difference between the source area and slope toe was about 240 m (Figure 2).

Lithology

Permian and Triassic strata were exposed from south to north in the study area (Figure 2). The Permian Longtan Formation (P_2lt) is composed of gray medium-thick mudstone sandwiched with green–gray medium-thick lithic sandstone, siltstone, dark gray limestone, and siliceous sandstone. The overlying strata consist of the lower Triassic Feixianguan Formation, which are mainly distributed in the foothills of Zongling Town. The rock formation attitude is 330°∠32°. There are two sections of the Triassic Feixianguan Formation. The first section (T_1f_1) is composed of medium-thick chlorotic siltstone (gray–green and dark purple), argillaceous calcareous siltstone, and mudstone (purple and gray–green) interbedded with silty mudstone, which is mainly

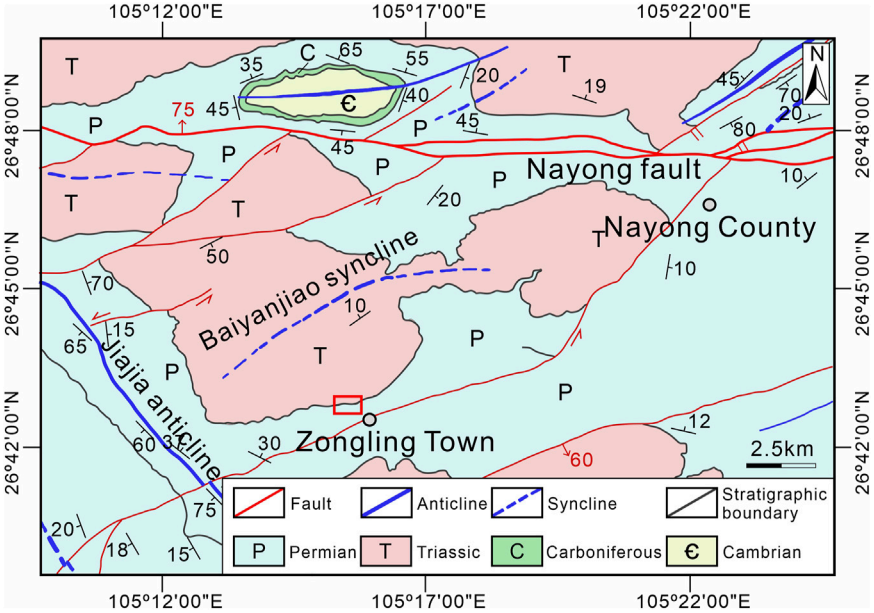

FIGURE 3
Regional tectonic and lithology map (modified from the work of Wu et al., 2019).

distributed in the middle upper cliff. The second section (T_1f_2) consists of thin–thick fine sandstone (gray–purple and green), calcareous sandstone, and basaltic lithic sandstone sandwiched with mudstone (purple), silty mudstone, thin–thick siltstone, tuff feldspar siltstone, silty limestone, and marl.

Regional tectonics

Folds and faults dominate the regional geological structures of the study site (Wu et al., 2019). The investigation area is located in the northeast wing of the Jiajia anticline and the south wing of the Baiyanjiao syncline, which belong to the northeast trending tectonic deformation area in the Bijie of Yangtze paraplatform. Northeast–southwest strike–slip faults are developed in the intermontane basin south of the rockfall. The Nayong fault is located about 13 km to the northwest (Figure 3). Due to the influence of tectonic activity, joints and fissures are developed in the limestone, and Figure 4A shows the scratches and steps left by tectonic action after a joint had been filled with calcite. Two groups of fissures are developed mainly in the western region, with attitude of 200–253°∠52–70° and 53–145°∠70–80° and a fracture rate of 1–4/m. Two groups of fractures are developed mainly in the eastern region, with the occurrence rates of 200–315°∠60–80°and 50–145°∠55–85° and fracture rates of 1–7/m. The two groups of joints in the east and west cut the limestone into vertical blocks, causing the formation of dominant open fractures near the outcrop (Shen and Li, 2015; Cheng et al., 2019; Wu et al., 2019).

Human activity

The main human activity related to the geodisaster at the study site was coal mining (Xiao et al., 2018). Along the rockfall zone in Zongling Town, there were more than 10 licensed coal mines (Tan, 2013). In 2004, 44 people were killed during the Zuojiaying landslide in the Zongling rockfall zone. Mining activity was the major triggering factor for this catastrophic landslide, and there were five coal mines near the landslide: Zhongling Mine, Zuojingying Mine, Sunxiao Mine, Xingyi Mine, and Huangjiagou Mine (Chen et al., 2006). Recently, these coal mines were shut down due to the continuous deformation and failure of slopes (Figure 4). However, large previously mined-out areas will continue to affect the integrity of the mountain structure in this area.

Meteorological and hydrographic characteristics

The study region is located in the subtropical warm and humid zone. It has an average annual temperature of 13.6°C and an average annual precipitation of 1,243.5 mm, mainly

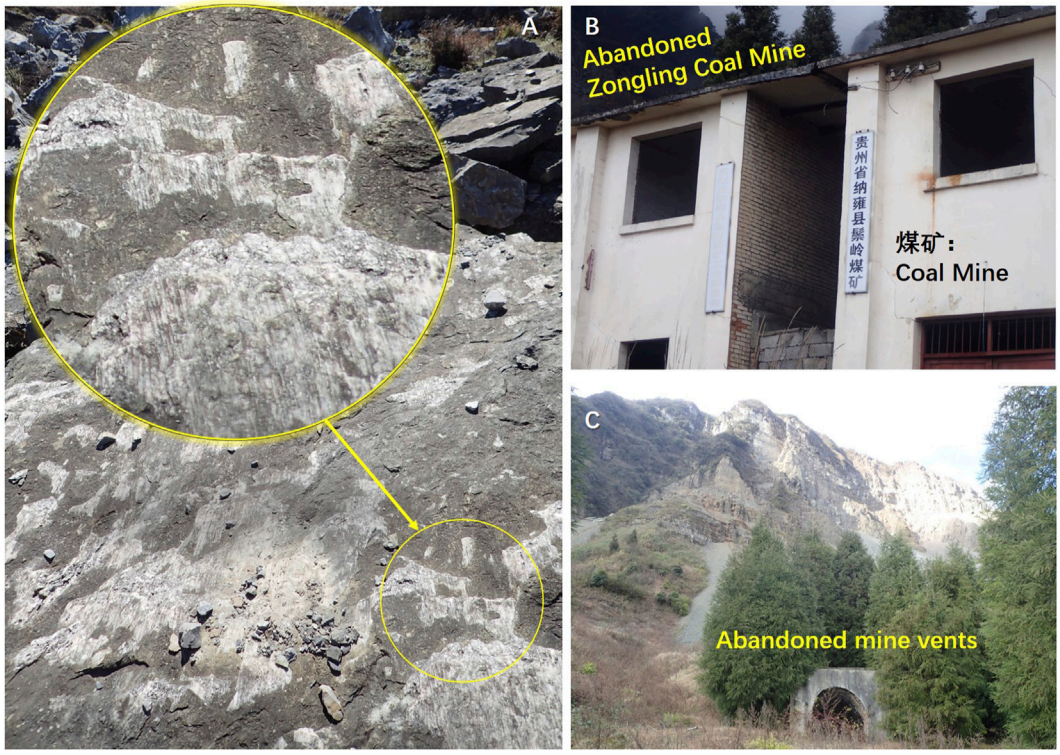

FIGURE 4
Tectonic indications **(A)** and human activity (**(B)** and **(C)**) at the study site.

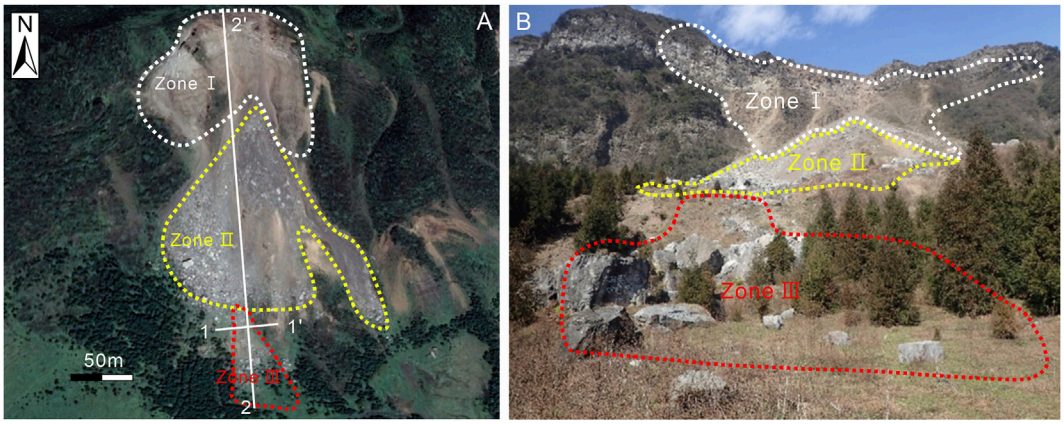

FIGURE 5
Overall features of the rockfall-dominated talus slope: **(A)** plane view (image source: Google Earth) and **(B)** front view.

from May to October, which accounts for about 70% of the annual precipitation (Cheng et al., 2019). The study site is located in the north and west of the Guizhou Plateau, which belongs to the Wujiang River basin in the Yangtze River system (Shen and Li, 2015). The main condition of groundwater is fissures water. Rainfall is the main groundwater recharge at this specific study site. In the upper part of the slope, with a larger topographic cut

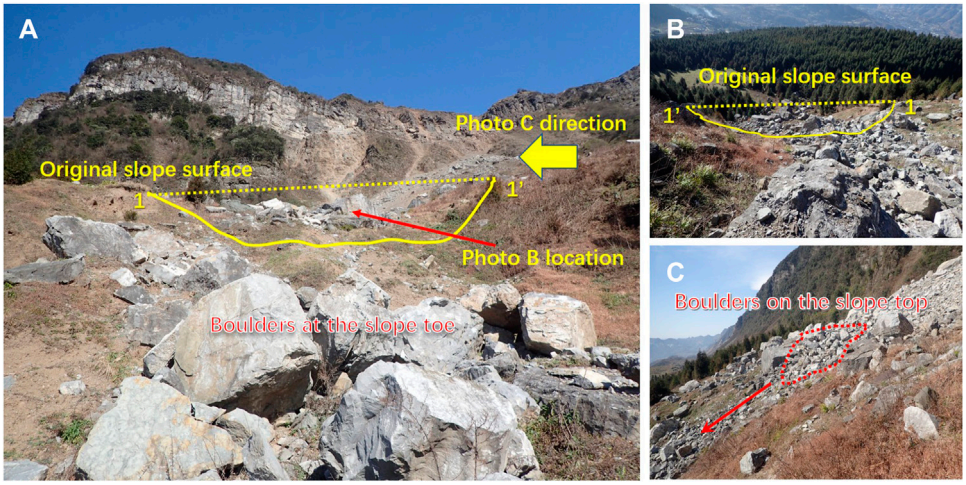

FIGURE 6
Detailed geomorphic features and boulder distribution of the failure area (Zone III). **(A)** overview of failure area, **(B)** boulders in the landslide trough, and **(C)** boulders on the slope top.

depth, the recharge, runoff, and discharge of groundwater alternate quickly, and the connection between the aquifers is poor.

Rockfall-dominated talus slope

The general morphology of this rockfall-dominated talus slope is fan-shaped in the plane. It is about 400 m long from north to south and 240 m wide from east to west. The orientation of the collapse direction is south-forward. Based on its morphology and material composition, this outcrop–talus system can be divided into the outcrop area (Zone I), talus slope (Zone II), and failure area (Zone III) (Figure 5).

Zone I is located at a cliff with a height of 50 m (Figure 5A). The bedrock at the lower cliff is gray–green, medium-thick siltstone interbedded with thin mudstone. The bedrock at the upper cliff is gray–green, medium-thick, fine sandstone interbedded with marl. The stratum inclines into the slope. The rock mass is cut into blocks of different sizes by joints.

Zone II is below the outcrop area. The height of the talus slope is about 120 m. The width of dispersion was about 180 m from west to east (Figure 5B). The slope angle is about 40° in the middle and upper parts. Gradually, the slope angle is reduced to 10° in the lower part. A platform is connected to the toe of the talus slope. The cone is mainly composed of gravel and residual soil with certain sorting properties. It presents fine debris at the top of the slope cone and boulders on the platform.

The failure area (Zone III) is below the platform of the talus slope (Figure 5) with a southern sliding direction. Figure 6 shows the detailed geomorphic features of the collapse area. The photo in Figure 6A was taken at the slope toe. The dotted line area represents the original slope surface before slope failure. Then, there is a landslide trough with an average depth of 3 m after the slope failure. The width of the sliding body was about 15 m. The length of the sliding mass was about 100 m. The western boundary of the landslide shows a steep slope with a slope angle of 55° and a height of 2 m, while the eastern boundary presents a steep shape. A large volume of boulders can be seen deposited at the slope toe. In Figure 6B, taken from the slope top to the slope toe along the sliding direction, it is evident that boulders were distributed in the landslide. Figure 6C indicates the western orientation at the slope top, where there are a few large boulders (delineated by the red dotted line). Those missing large boulders are situated in the landslide trough and at the toe of the slope in Figure 6A.

Due to differential weathering, there is a cavity below the unstable rock mass in the source area (Figure 7A). The stereographic projection analysis of rock mass in the source area of collapse was carried out using the occurrence data (Table 1) of the rock strata and joints obtained from the investigation. The rock layer has been cut into blocks by J_1, J_2, J_3, and J_4 joints. The intersecting lines of J_2 and P_1 and of J_4 and P_1, which are the main controlling structural planes, tend toward the outside of the slope, and their inclination is less than the slope angle. The intersection lines of the other combinations tend toward the inside of the slope. Thus, although the rock mass in the source area is relatively fragmented, the whole rock mass is in a stable state, and only some boulders close to the slope are unstable. In extreme cases, such as earthquakes and torrential rain, fractures may expand the trend, and the dangerous rock mass may slide and collapse downward.

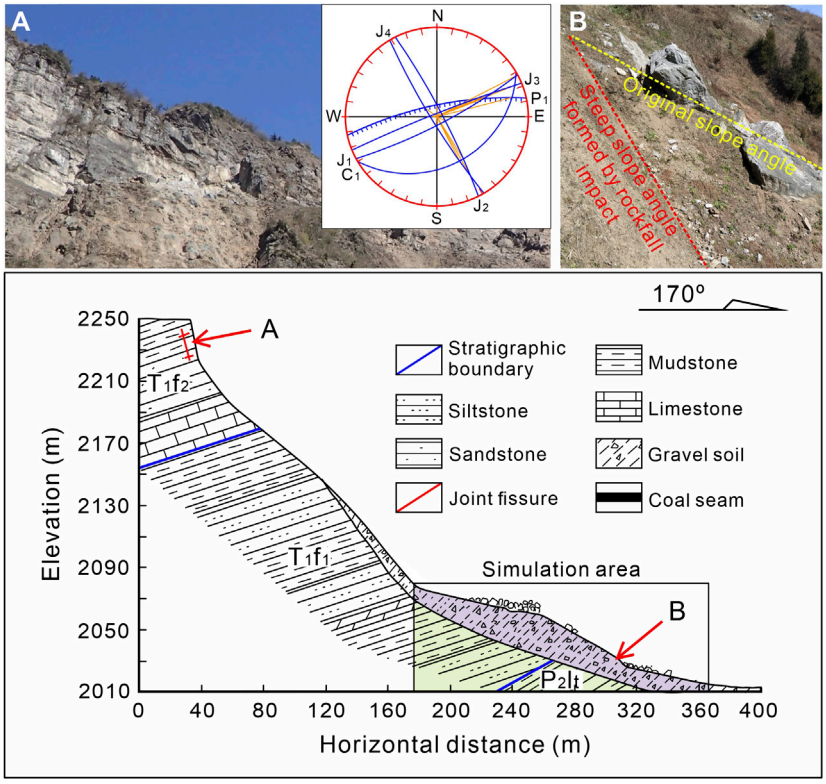

FIGURE 7
Profile section 2-2′ of this rockfall-dominant talus slope. **(A)** source area and **(B)** slope toe cutting by rockfall impact.

TABLE 1 Parameters for stereographic projection.

Notation	Structural plane	Dip direction (°)	Dip angle (°)
P_1	Slope surface	168	75
C_1	Bedding plane	330	32
J_1	Joint 1	59	83
J_2	Joint 2	332	83
J_3	Joint 3	243	83
J_4	Joint 4	158	86

About 5 m west of the western boundary of the collapse area, there is an impact trace formed by a recent rockfall. The fallen boulder was 2.5 m long, 2 m wide, and 2.3 m high. The upper slope angle of the slope body was about 35°. The lower slope angle of the slope body was about 60°, and the development of a small slope was about 2.5 m high (Figure 7B). Based on the rockfall trajectory, it appears that the slope change was caused mainly by the impact, scraping, and pushing of the lower part of the slope body when the rockfall impacted the toe of slope.

Figure 8 shows the ground traces located near the slope toe of the collapse area after the rockfall impact. The green zone indicates a long trench created by the boulder scraping action, the blue zone highlights the sidewall of the long trench, and the red zone shows a steep main scarp near the ground traces. It is evident that the geometry of the slope changed after the rockfall impact, so it may be concluded that frequent rockfall events induce toe cutting, which contributes to slope instability.

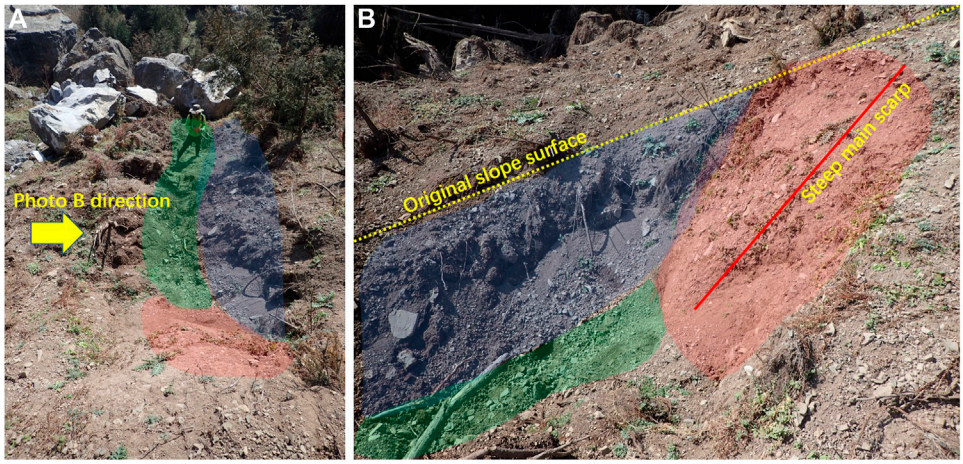

FIGURE 8
Slope toe cutting by rockfall impact: **(A)** view toward slope toe and **(B)** side view.

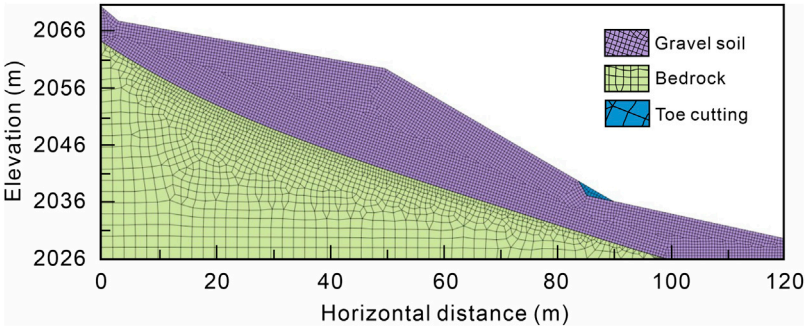

FIGURE 9
Numerical model for SRM.

Effects of top loading and toe cutting on slope stability

One objective of the study was to analyze how boulder load at the top of the slope and slope cutting at the slope toe contribute to landslide formation. Thus, the failure area (see Figure 7), including the platform and toe of the talus slope, was selected as the geological model for numerical simulation. To reduce the influence of boundary range conditions on calculation errors and to improve the calculation accuracy, the size of the model (Figure 9) was set as the distance from the slope toe to the left edge at 1.5 times the slope height, the distance from the top to the right edge was set to 2.5 times the slope height, and the total height of the upper and lower edges was set to no less than two times the slope height (Zhao et al., 2002; Zheng et al., 2002). MIDAS/GTS software was used to carry out the slope stability analysis under the following conditions: a) without top loading and toe cutting, b) top loading, c) toe cutting, and d) top loading and toe cutting. The numerical model (Figure 9) was established based on the field investigations and previous research on the Zongling rockfall (Chen et al., 2006). The slope material structure can be divided into two layers: the upper is gravel soil and the lower is bedrock. The basic physical and strength parameters of the gravel soil and bedrock, shown in Table 2, were obtained from a comprehensive review of field geological surveys, laboratory tests, and relevant regional experience (Chen et al., 2006; Cheng et al., 2019). The slope stability was analyzed using the finite element strength reduction method (SRM).

TABLE 2 Physical and mechanical parameters of soil and rock martials.

Parameters	Unit weight, γ (kN/m^3)	Elasticity modulus, E (MPa)	Poisson's ratio, ν	Cohesion c, (kPa)	Internal friction angle, φ (°)
Gravel soil	21.2	60	0.31	10.5	22.1
Bedrock	25	650	0.4	32	59

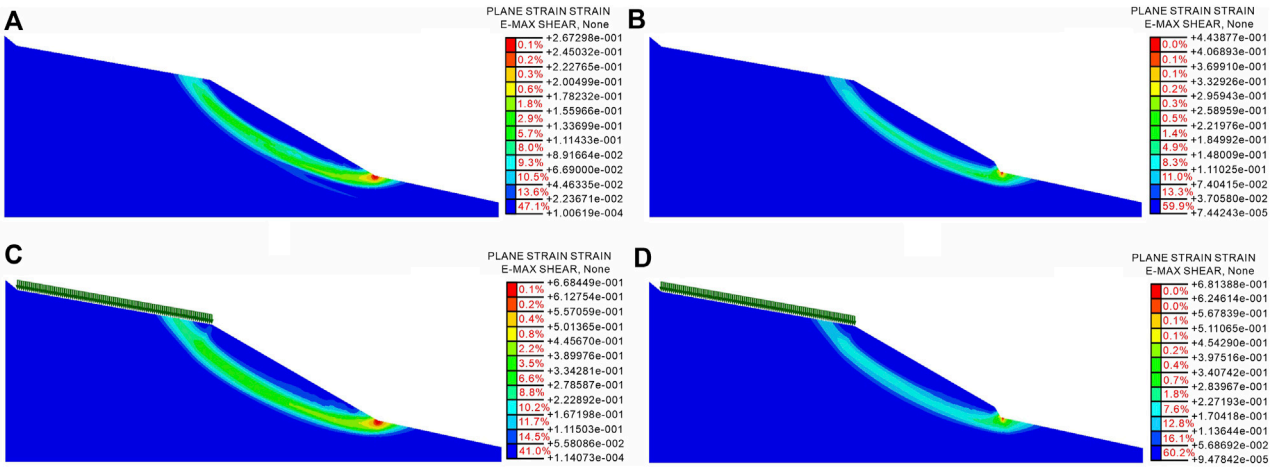

FIGURE 10
Maximum shear strain for four conditions: **(A)** without top loading and toe cutting, **(B)** toe cutting, **(C)** top loading, and **(D)** top loading and toe cutting.

The top loading simulation was located at the top of the slope. The density of the overlying boulders was 2,200 kg, and the thickness was 2 m. Therefore, the linear uniform load can be calculated as 43.12 kN/m. The toe cutting state simulates the phenomenon of slope cutting caused by rockfalls impacting the slope toe, as observed in the lower part of the collapse zone. The slope angle after cutting the slope was set to 60°. All materials were subjected to the Mohr–Coulomb failure criteria.

The numerical simulation results show that the maximum plastic deformation is concentrated at the toe of the slope for four simulation conditions (Figure 10). The safety factors of the slopes under conditions A, B, C, and D were 1.11, 1.06, 1.10, and 1.04, respectively. Theoretically, the slope is stable. However, in engineering practice, to make sure the slope has enough of a safety reserve, it is generally considered that the slope with a safety factor of Fs = 1.1–1.5 is stable. Therefore, the slopes in these four states are near the critical state of instability. The safety factor of the slope for the top loading condition was 0.01 smaller than that for the non-top loading and non-toe cutting conditions. The results indicate that boulders loading on the top of the slope has some influence on the stability of the slope, but that effect is not significant. The safety factor of slope for toe cutting condition was 0.05 smaller than that for the non-top loading and non-toe cutting conditions. Here, the results indicate that the rockfall impact at the toe of the slope has a significant influence on the stability of the slope. The effect of toe cutting on slope stability was greater than that of top loading. The safety factor of the slope under the combined action of top loading and toe cutting was 0.07 smaller than for the non-top loading and non-toe cutting conditions. This result indicates that the slope becomes more unstable under the combined action of rockfalls.

Formation mechanism and failure mode

The lithology and rock mass structure of the study site are the controlling factors for outcrop retreat and the progressive development of talus deposits. The upper part of the outcrop slope is limestone, and the lower part is siltstone and mudstone with the overall structure of the slope being hard at the top and soft at the bottom. Siltstone and mudstone can occur the differential weathering during the wetting and drying cycles due to rainfall and Sun exposure (Chen et al., 2006; Lo, 2015).

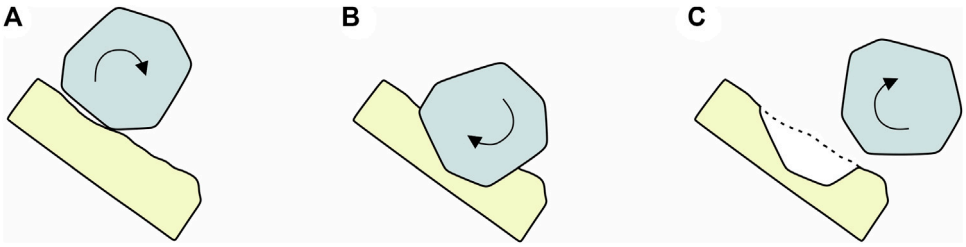

FIGURE 11
Process diagram of the rockfall impact on the talus slope **(A)** contact, **(B)** impact, and **(C)** rebound.

Differential weathering appeared on the outcrop (Figure 7A), and regional tectonics, such as the Baiyanjiao syncline and the Jiajia anticline, controlled the development of joints and fissures on the slope. Due to the long-term geological action, cracks in the rock mass were gradually connected and enlarged to separate the slope surface rock mass from the bedrock. At the same time, weathering, dissolution, and surface water infiltration along the fissure also cause the fissure to expand further and gradually extend downward to form a complete fissure.

Rainfall and human activity are the main external influencing factors on slope stability (Dong et al., 2015; Cheng et al., 2019). The rainfall in the study area was relatively concentrated. On one hand, precipitation infiltration into the unloading cracks causes an increase in water pressure. On the other hand, the rock mass itself presents a structure that is hard at the top and soft at the bottom, and the infiltration of precipitation results in a decrease in the lower, weaker rock stratum's falling strength. Due to the dual action of water filling the unloading fissure and softening the base, the stability of the rock mass is eventually reduced. The slope deformation was further aggravated by long-term mining engineering. The ground collapse and mountain cracking in this area are mainly caused by large goaf areas, long mining times, and shallow buried mining areas (Tan, 2013). The cracks at the top of the mountain have opened about 1–2 m wide, and some blocks have been separated and even became isolated from the bedrock. More importantly, the cracks in the mountain show a developing trend, which may progress quite easily and cause a large-scale mountain collapse. When mining reaches a certain scale, a large area of goaf deformation occurs. The blast loading and mining collapse of human activity eventually degrade the integrity of the rock mass (Xiao et al., 2018). Thus, because the buried depth is shallow, the deformation zone will affect the surface rock mass, and the slope will crack accordingly.

The detached boulders and fragments provide a continuous source of materials for the evolution of this talus slope and gradually change the slope geometry over time. The boulders accumulated on the top of the slope for a long time and continued to load in the upper part of the slope, resulting in creeping deformation of the slope body. In addition, a large boulder on the talus slope reduced the angle of the slope (Evans and Hungr, 1993). Moreover, slope microtopography affected the movement characteristics of the rockfall (Imaizumi et al., 2020; Collins et al., 2022). The relatively flat terrace (Figure 7B) in the middle section of the talus slope increases the jump height of the boulders. The collision process between the beginning of the rockfall and its terminus can be divided into several stages (Dorren et al., 2004; Lu et al., 2019). Figure 11 illustrates the process diagram of the rockfall impact on the talus slope, which

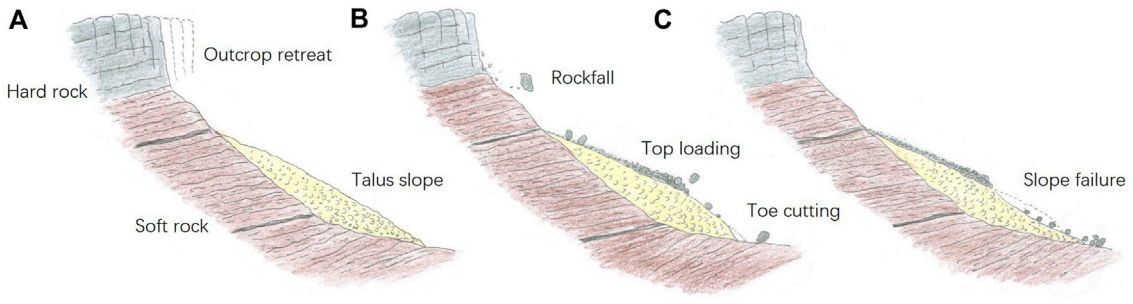

FIGURE 12
Schematic diagram of the formation mechanism and failure mode of a talus slope induced by rockfalls. **(A)** outcrop retreat, **(B)** top loading and toe cutting, **(C)** slope failure.

includes the contact, impact, and rebound stages. After the last stage, the rolling boulder remains as a trace on the slope and functions as a toe cutting (Figure 8). According to the numerical simulation analysis, toe cutting has a great influence on slope stability.

The failure mode of the talus slope induced by rockfalls at this study site is illustrated in Figure 12. The regional tectonic activities control the development of rock joints and fissures. The lithology—hard upper and soft lower at the outcrop—leads to differential weathering. External factors, such as goaf deformation and rainfall, aggravate the development of rock fissures. Frequently, the boulders detach, and these fragments cause the outcrop to retreat, along with the progressive development of talus deposits (Figure 12A). The boulders deposit on the platform in the middle section of the talus slope, which then serves as top loading for the slope mechanical system (Figure 12B). During the boulder–ground interaction of a rolling boulder with a high jump, the rockfall impact functions as a form of toe cutting to change the geometry of the talus slope. The mechanical balance of the slope changes at the same time, which causes a decrease in the antisliding force of the slope. Finally, on this talus slope, slope failure occurred due to the combined effect of top loading and toe cutting (Figure 12C). It is therefore evident that the prevention and mitigation efforts in this region should pay close attention to the role of rockfall impact in the geodisaster chain that affects talus slopes, while also considering the more commonly understood rockfall trajectory.

Conclusion

(1) The Zongling rockfall zone is one of the most active outcrop–talus slope systems in southwest China. The lithology and rock mass structure of the study site are the controlling factors for the outcrop retreat and the progressive development of talus deposits. The external influencing factors of rainfall and human activities enhance this process.
(2) Boulder accumulation on the platform in the middle section of the talus slope functions as top loading for the slope mechanical system. During the boulder-ground interaction, the rockfall impact causes toe cutting to change the geometry and mechanical balance of the talus slope. It was found that toe cutting has a significant influence on slope stability, which then leads to a decrease in the antisliding force of the talus slope. The slope failure induced by rockfalls then occurs due to the combined effect of top loading and toe cutting on this talus slope.
(3) In this region, a rockfall geodisaster event may trigger a large-scale slope failure as one outcome of the geodisaster chain. Therefore, the prevention and mitigation efforts in this region should pay close attention to the role of rockfall impact in the specific geodisaster chains that affect talus slopes, while also considering the more commonly understood rockfall trajectory.

Data availability statement

The original contributions presented in the study are included in the article/Supplementary Material. Further inquiries can be directed to the corresponding author.

Author contributions

HY: conceptualization, methodology, data curation, writing—original draft, and formal analysis. BX: conceptualization, methodology, and formal analysis. JH: conceptualization, methodology, and formal analysis. HJ: conceptualization, methodology, and formal analysis. QC: conceptualization, methodology, and formal analysis.

Funding

This work was supported by the Sichuan Science and Technology Program (Grant No. 2022YFG0141) and National Natural Science Foundation of China (Grant No. 41807248).

Conflict of interest

Author HJ was employed by the company Kunming Survey, Design, and Research Institute Co., Ltd., of CREEC. Author QC was employed by the company Sichuan Highway Planning, Survey, Design, and Research Institute Ltd.

The remaining authors declare that the research was conducted in the absence of any commercial or financial relationships that could be construed as a potential conflict of interest.

Publisher's note

References

Chen, Z. F., Kong, J. M., and Wang, C. H. (2006). Characteristics of the falling-slide type landslide in Nayong in Guizhou Province and the lessons learned for disaster mitigation in other areas. *Chin. J. Geol. Hazard Control* 17, 32–35. doi:10.3969/j.issn.1003-8035.2006.03.008

Cheng, Y., Zhang, J., Chen, J., and Long, J. (2019). Analysis on stability and hazard zone of dangerous rock mass in zongling Town, Nayong of Guizhou Province. *Chin. J. Geol. Hazard Control* 30 (4), 9–15. doi:10.16031/j.cnki.issn.1003-8035.2019.04.02

Collins, B. D., Corbett, S. C., Horton, E. J., and Gallegos, A. J. (2022). Rockfall kinematics from massive rock cliffs: Outlier boulders and flyrock from whitney portal, California, rockfalls. *Environ. Eng. Geosci.* 28 (1), 3–24. doi:10.2113/EEG-D-21-00023

Colucci, R. R., Boccali, C., Žebre, M., and Guglielmin, M. (2016). Rock glaciers, protalus ramparts and pronival ramparts in the south-eastern Alps. *Geomorphology* 269, 112–121. doi:10.1016/j.geomorph.2016.06.039

Curry, A. M., and Morris, C. J. (2004). Lateglacial and holocene talus slope development and rockwall retreat on mynydd du, UK. *Geomorphology* 58 (1–4), 85–106. doi:10.1016/S0169-555X(03)00226-5

De Blasio, F. V., and Sæter, M. B. (2015). Dynamics of grains falling on a sloping granular medium: Application to the evolution of a talus. *Earth Surf. Process. Landforms* 40, 599–609. doi:10.1002/esp.3655

Dong, X. J., Pei, X. J., and Huang, R. Q. (2015). The longchangzhen collapse in kaili, Guizhou: Characteristics and failure causes. *Chin. J. Geol. Hazard Control* 26 (3), 3–9. doi:10.16031/j.cnki.issn.1003-8035.2015.03.02

Dorren, L. K. A., Maier, B., Putters, U. S., and Seijmonsbergen, A. C. (2004). Combining field and modelling techniques to assess rockfall dynamics on A protection forest hillslope in the European Alps. *Geomorphology* 57 (3–4), 151–167. doi:10.1016/S0169-555X(03)00100-4

Evans, S. G., and Hungr, O. (1993). The assessment of rockfall hazard at the base of talus slopes. *Can. Geotech. J.* 30 (4), 620–636. doi:10.1139/t93-054

Gerber, E., and Scheidegger, A. E. (1974). On the dynamics of scree slopes. *Rock Mech.* 6 (1), 25–38. doi:10.1007/bf01238051

Gong, X. X., and Zhao, X. (2009). Type, causation and prevention of geologic disaster hidden danger in Nayong county. *Guizhou Geol.* 26 (3), 235–237. doi:10.3969/j.issn.1000-5943.2009.03.019

Hale, A. J., Calder, E. S., Loughlin, S. C., Wadge, G., and Ryan, G. A. (2009). Modelling the lava dome extruded at soufriere hills volcano, Montserrat, august 2005-may 2006 Part II: Rockfall activity and talus deformation. *J. Volcanol. Geotherm. Res.* 187 (1–2), 69–84. doi:10.1016/j.jvolgeores.2009.08.014

Hendrickx, H., Lars, D. S., Cornelis, S., Reynald, D., Jan, N., and Amaury, F. (2020). Talus slope geomorphology investigated at multiple time scales from high-resolution topographic surveys and historical aerial photographs (sanetsch pass, Switzerland). *Earth Surf. Process. Landforms* 45 (14), 3653–3669. doi:10.1002/esp.4989

Imaizumi, F., Trappmann, D., Matsuoka, N., Cánovas, J. A. B., Yasue, K., and Stoffel, M. (2020). Interpreting rockfall activity on an outcrop–talus slope system in the southern Japanese Alps using an integrated survey approach. *Geomorphology* 371, 107456. doi:10.1016/j.geomorph.2020.107456

Jiao, W. (2015). Analysis on Stopping area and influencing Factors of typical dangerous rock collapse, *master's thesis*. Guiyang, China: Guizhou University.

Jomelli, V., and Francou, B. (2000). Comparing the Characteristics of Rockfall Talus and Snow Avalanche Landforms in an Alpine Environment Using a New Methodological Approach: Massif des Ecrins, French Alps. *Geomorphology* 35 (3–4), 181–192. doi:10.1016/S0169-555X(00)00035-0

Liu, C. Z., Guo, Q., and Chen, H. Q. (2004). Preliminary analysis on the cause of dangerous rock collapse in yanjiaozhai, Nayong county, Guizhou Province. *Chin. J. Geol. Hazard Control* 15, 123+144. doi:10.3969/j.issn.1003-8035.2004.04.029

Lo, C. M. (2015). Cliff retreat and progressive development of talus deposits in hungtsaiping rockfall area, NanTou, taiwan. *Landslides* 12, 29–54. doi:10.1007/s10346-013-0459-4

Lu, G., Caviezel, A., Christen, M., Demmel, S. E., Ringenbach, A., Bühler, Y., et al. (2019). Modelling rockfall impact with scarring in compactable soils. *Landslides* 16, 2353–2367. doi:10.1007/s10346-019-01238-z

Matsuoka, N., and Sakai, H. (1999). Rockfall activity from an alpine cliff during thawing periods. *Geomorphology* 28 (3-4), 309–328. doi:10.1016/S0169-555X(98)00116-0

McCarroll, D., Shakesby, R. A., and Mattews, J. A. (2001). Enhanced rockfall activity during the little ice age: Further lichenometric evidence from a Norwegian talus. *Permafr. Periglac. Process.* 12 (2), 157–164. doi:10.1002/ppp.359

Messenzehl, K., Viles, H., Otto, J. C., Ewald, A., and Dikau, R. (2018). Linking rock weathering, rockwall instability and rockfall supply on talus slopes in glaciated hanging valleys (Swiss Alps). *Permafr. Periglac. Process.* 29 (3), 135–151. doi:10.1002/ppp.1976

Otto, J. C., and Sass, O. (2005). Comparing geophysical methods for talus slope investigations in the turtmann valley (Swiss Alps). *Geomorphology* 76 (3–4), 257–272. doi:10.1016/j.geomorph.2005.11.008

Sanders, D. (2010). Sedimentary facies and progradational style of a pleistocene talus-slope succession, northern calcareous Alps, Austria. *Sediment. Geol.* 228 (3–4), 271–283. doi:10.1016/j.sedgeo.2010.05.002

Sanders, D., Widera, L., Ostermann, M., and Baas, J. (2014). Two-layer scree/snow-avalanche triggered by rockfall (eastern Alps): Significance for sedimentology of scree slopes. *Sedimentology* 61 (4), 996–1030. doi:10.1111/sed.12083

Sass, O., and Krautblatter, M. (2007). Debris flow-dominated and rockfall-dominated talus slopes: Genetic models derived from GPR measurements. *Geomorphology* 86 (1–2), 176–192. doi:10.1016/j.geomorph.2006.08.012

Shen, T. Q., and Li, J. Y. (2015). Study on formation mechanism of collapse in zongling Town, Guizhou Province. *Technol. Innov. Appl.* 35, 19–20.

Shi, Y. S. (2019). Risk Assessment and Management of Rockslide in the rural area - a case Study in zongling Town, Guizhou, *master's thesis*. China, Sichuan, Chengdu: Chengdu University of Technology. doi:10.26986/d.cnki.gcdlc.2019.000412

Statham, I. (1976). A scree slope rockfall model. *Earth Surf. Process.* 1 (1), 43–62. doi:10.1002/esp.3290010106

Tan, N. (2013). Failure Mechanism and stability Evaluation of the zhongling high slope Deformation on mine Area in Nayong county, *master's thesis*. China, Sichuan, Chengdu: Chengdu University of Technology.

Vehling, L., Baewert, H., Glira, P., Moser, M., Rohn, J., and Morche, D. (2017). Quantification of sediment transport by rockfall and rockslide processes on a proglacial rock slope (kaunertal, Austria). *Geomorphology* 287, 46–57. doi:10.1016/j.geomorph.2016.10.032

Veilleux, S., Bhiry, N., and Decaulne, A. (2020). Talus slope characterization in tasiapik valley (subarctic québec): Evidence of past and present slope processes. *Geomorphology* 349, 106911. doi:10.1016/j.geomorph.2019.106911

Wan, Y. H., Zhao, X. Y., Ling, S. X., Li, J., Zeng, C. Y., and Bernd, W. (2021). Directional arrangement of phyllite fragments in phyllite talus slope at the eastern margin of the Tibetan plateau. *J. Mt. Sci.* 18 (11), 3069–3081. doi:10.1007/s11629-020-6605-2

Wang, J. (2019). Study on Damage and Deformation of slope rock mass Caused by underground goaf, *master's thesis*. China, Sichuan, Chengdu: Chengdu University of Technology. doi:10.26986/d.cnki.gcdlc.2019.000827

Wu, C. Y., Qiao, J. P., Wang, C. H., Kong, J. M., and Chen, Z. F. (2006). Analysis on "12·3" super large-scaled landslide in zongling, Nayong, Guizhou. *Res. Soil Water Conserv.* 13 (6), 100–102. doi:10.3969/j.issn.1005-3409.2006.06.031

Wu, K. B., Jiang, K. Y., Huang, W. J., Yue, L. H., and Zhang, D. M. (2019). Tectonic formation features and its evolution in nayong-shuicheng area of northwest Guizhou. *Guizhou Geol.* 36 (2), 165–172. doi:10.3969/j.issn.1000-5943.2019.02.009

Xiao, R. H., Chen, H. Q., Leng, Y. Y., Wei, Y. J., and Wang, W. P. (2018). Preliminary analysis on the failure process and mechanism of the august 28 collapse in Nayong county Guizhou Province. *Chin. J. Geol. Hazard Control* 29 (1), 3–9. doi:10.16031/j.cnki.issn.1003-8035.2018.01.02

Xing, H. F., Liu, L. L., and Luo, Y. (2019). Water-induced changes in mechanical parameters of soil-rock mixture and their effect on talus slope stability. *Geomech. Eng.* 18 (4), 353–362. doi:10.12989/gae.2019.18.4.353

Zhang, Y. C., Huang, R. Q., Fu, R. H., and Pei, X. J. (2010). Experimental research on dynamic failure mechanism of large-scale talus slope. *Chin. J. Rock Mech. Eng.* 29 (1), 65–72.

Zhao, S. Y., Zheng, Y. R., Shi, W. M., and Wang, J. L. (2002). Analysis on safety factor of slop by strength reduction FEM. *Chin. J. Geotech. Eng.* 24 (3), 343–346. doi:10.3321/j.issn:1000-4548.2002.03.017

Zheng, Y. R., Zhao, S. Y., and Zhang, L. Y. (2002). Slope stability analysis by strength reduction FEM. *Eng. Sci.* 4, 57–61+78. doi:10.3969/j.issn.1009-1742.2002.10.011